

15 Jan 2023

## Network Structures and the Properties of Na-Ca-Sr-Borophosphate Glasses

Parker T. Freudenberger

Rebekah L. Blatt

Randall E. Youngman

Richard K. Brow

Missouri University of Science and Technology, [brow@mst.edu](mailto:brow@mst.edu)

Follow this and additional works at: [https://scholarsmine.mst.edu/math\\_stat\\_facwork](https://scholarsmine.mst.edu/math_stat_facwork)

 Part of the [Materials Science and Engineering Commons](#)

---

### Recommended Citation

P. T. Freudenberger et al., "Network Structures and the Properties of Na-Ca-Sr-Borophosphate Glasses," *Journal of Non-Crystalline Solids*, vol. 600, article no. 121966, Elsevier, Jan 2023.

The definitive version is available at <https://doi.org/10.1016/j.jnoncrysol.2022.121966>

This Article - Journal is brought to you for free and open access by Scholars' Mine. It has been accepted for inclusion in Mathematics and Statistics Faculty Research & Creative Works by an authorized administrator of Scholars' Mine. This work is protected by U. S. Copyright Law. Unauthorized use including reproduction for redistribution requires the permission of the copyright holder. For more information, please contact [scholarsmine@mst.edu](mailto:scholarsmine@mst.edu).



# Network structures and the properties of Na-Ca-Sr-borophosphate glasses

Parker T. Freudenberger<sup>a</sup>, Rebekah L. Blatt<sup>a</sup>, Randall E. Youngman<sup>b</sup>, Richard K. Brow<sup>a,\*</sup>

<sup>a</sup> Department of Materials Science and Engineering, Missouri University of Science and Technology, Rolla, MO, United States

<sup>b</sup> Science & Technology Division, Corning Incorporated, Corning, NY, United States

## ARTICLE INFO

### Keywords:

Glasses  
Phosphate  
Borate  
Borophosphate  
Structure  
High pressure liquid chromatography  
Nuclear magnetic resonance  
Raman spectroscopy

## ABSTRACT

Borophosphate glasses were prepared with the nominal molar compositions  $16\text{Na}_2\text{O}-(24-y)\text{CaO}-y\text{SrO}-x\text{B}_2\text{O}_3-(60-x)\text{P}_2\text{O}_5$  (mol%), where  $0 \leq x \leq 60$  and  $y=0, 12$ , and  $24$ . Information about the compositional dependence of borate and phosphate site speciation and next nearest neighbor linkages was obtained by  $^{11}\text{B}$  and  $^{31}\text{P}$  MAS NMR and Raman spectroscopies, and by high pressure liquid chromatography (HPLC). With the initial replacement of  $\text{P}_2\text{O}_5$  by  $\text{B}_2\text{O}_3$ , tetrahedral borate sites linked to four phosphate anions,  $\text{B}(\text{OP})_4$ , are created in the glass structure, and the average phosphate anion becomes smaller as bridging P $\text{OP}$  bonds are replaced by bridging P $\text{OB}$  bonds. With further increases in the  $\text{B}_2\text{O}_3$  content, borate units, including B-triangles, replace phosphate units linked to the B-tetrahedra. Compositional trends for the glass transition temperature ( $T_g$ ) and molar volume are explained by considering the number and types of bridging oxygens per glass former, consistent with topological models reported elsewhere.

## 1. Introduction

Borophosphate glasses have been developed for a wide variety of applications, including their use in biomedical, optical, and energy storage devices [1–7]. Small additions of borate to phosphate glass increase thermal stability [3,8,9], reduce a tendency towards devitrification [3,5] and decrease dissolution rates in aqueous solutions [1,2,5]. The ionic conductivity of alkali borophosphate glasses has a nonlinear dependence on composition when borate replaces phosphate, and this behavior has been called the “mixed glass-former effect” [4,10].

The structures of the borophosphate glasses have been studied by a variety of techniques, including several different nuclear magnetic resonance (NMR) experiments; e.g., magic angle spinning (MAS), multiple quantum magic angle spinning (MQMAS), heteronuclear correlation (HETCOR), and rotational echo double resonance (REDOR) [4, 10–13]. These studies have shown that heteroatomic linkages are preferred in the structures of borophosphate glasses to maximize the number of B-O-P linkages per boron [9–13].  $^{31}\text{P}\{^{11}\text{B}\}$  and  $^{11}\text{B}\{^{31}\text{P}\}$  rotational echo double resonance (REDOR) spectra collected from alkali borophosphate glasses indicate a preference for phosphate species linked to two borate groups and another phosphate group [12]. Overall, these NMR studies reveal that for alkali borophosphate glasses, the anionic moieties that form with the systematic replacement of phosphate by borate occur in the order  $\text{B}^4 > \text{P}^2 > \text{P}^1 > \text{P}^0 > \text{B}^2 > \text{B}^1 > \text{B}^0$ ,

where the superscript indicates the number of bridging oxygens associated with the respective B- and P-sites [11,14].

Hermansen *et al.* [14,15] used information from similar structural studies with assumptions including the borate avoidance principal [16] to develop a topological model to predict the compositional dependences of the relative concentrations of the B- and P-sites that constitute the structures of phosphate and borophosphate glasses, and used this model to explain compositional trends in physical properties, including glass transition temperature ( $T_g$ ), Vicker’s hardness, melt fragility, and the isobaric heat capacity jump at  $T_g$ . The model was evaluated using information collected on borophosphate glasses with a variety of modifying oxides, including sodium, lithium, potassium, cesium, and calcium. The model considered the effects of glass formers and modifiers on network topology, although some modifications were required to account for the compositional dependence of the thermal properties of calcium borophosphate glasses [14].

Sodium calcium phosphate and borophosphate glasses have been developed for biomedical applications [3,7,17–21]. Strontium and calcium have similar physiological effects as they are both absorbed in the gastrointestinal tract, concentrated in bone, and excreted primarily in urine [22]. *In vivo* studies have shown that the substitution of strontium for calcium in different bioactive silicate-based glasses and ceramics stimulated osteoblasts to generate new bone and osteoclasts were prevented from resorbing bone, responses similar to those induced by

\* Corresponding author.

E-mail address: [brow@mst.edu](mailto:brow@mst.edu) (R.K. Brow).

strontium ranelate, a drug approved for the treatment and prevention of osteoporosis [23–25]. The substitution of strontium for calcium in sodium metaphosphate glasses decreased dissolution rates in water by over an order of magnitude and increased the refractive index while maintaining an acceptable difference in the coefficient of thermal expansion, properties designed to produce core-clad fibers with potential biomedical applications [26].

Many studies of the compositional dependence of the properties and structures of borophosphate glasses have been done on series where variations in the modifier contents affected the borate and phosphate site speciation [8,9,11,12,27,28]. In the present study, the modifier to glass former ratio is kept constant so that the effects of the systematic substitution of borate for phosphate on the structures and properties of Na-Ca-Sr-borophosphate glasses could be characterized using  $^{11}\text{B}$  and  $^{31}\text{P}$  MAS NMR, Raman spectroscopy, and high pressure liquid chromatography (HPLC). The structural information was analyzed using a modified version of the topological model proposed by Hermansen *et al.* [14] to explain the compositional trends in glass transition temperature and density. The effects of the composition and structure on the dissolution behavior of these glasses in water and in simulated body fluids are described in a separate paper [29].

## 2. Experimental procedure

Borophosphate glasses with the nominal molar compositions  $16\text{Na}_2\text{O}-(24-y)\text{CaO}-y\text{SrO}-x\text{B}_2\text{O}_3-(60-x)\text{P}_2\text{O}_5$ , where  $0 \leq x \leq 60$  and  $y=0, 12, \text{ and } 24$ , were prepared in 50g batches using  $\text{NaPO}_3$  (Shanghai Muhong Industrial Co., Ltd., Optical Grade),  $\text{Ca}(\text{PO}_3)_2$  (Shanghai Muhong Industrial Co., Ltd., Optical Grade),  $\text{H}_3\text{BO}_3$  (Fisher,  $\geq 99.5\%$ ),  $\text{Na}_2\text{CO}_3$  (Alfa Aesar, 99.5%),  $\text{CaCO}_3$  (Fisher,  $>98.0\%$ ),  $\text{SrCO}_3$  (Alfa Aesar, 97.5%) and  $\text{H}_3\text{PO}_4$ , 85% (Fisher, ACS Cert.) as raw materials. Powders were combined in a 150 mL Nalgene bottle and thoroughly shaken by hand before adding to a platinum crucible. When phosphoric acid was used as a raw material, it was added to the well-mixed dry components in the platinum crucible. Each batch was calcined at  $300^\circ\text{C}$  for four to twelve hours, depending on the composition, to evolve water from the batch materials. The batch was then melted at  $1000\text{--}1200^\circ\text{C}$  for one hour, stirred with a platinum rod after 30 minutes to promote homogeneity, and then cast into preheated graphite molds. The resulting glasses were annealed for one hour at  $350^\circ\text{C}$  before cooling to room temperature and then stored in a vacuum desiccator. Except for the  $x = 10$  composition in the CaO-free ( $y = 24$ ) series, glasses were transparent, colorless and confirmed to be fully amorphous by x-ray diffraction (XRD), using a PANalytical X'Pert Multipurpose diffractometer with a  $\text{Cu K}\alpha$  source and a PIXcel detector, and XRD was used to identify crystalline phases in melts that crystallized on quenching. The  $x = 10$  composition in the  $y = 24$  series was slightly gray in color but still transparent; this is assumed to be due to small amounts of platinum pickup during melting.

To determine glass compositions, 50mg of powders ( $<250\mu\text{m}$ ) were dissolved in 50mL of 3%  $\text{HNO}_3$  for up to one week. These solutions were then diluted to obtain three separate solutions having 1-50 ppm of the target ion concentrations, and these solutions were analyzed using inductively coupled plasma optical emission spectrometry (Perkin-Elmer Avio 200) to provide the average oxide compositions. Glasses are described throughout this manuscript using the analyzed  $\text{B}_2\text{O}_3$ -content.

Densities were measured using Archimedes' method, with deionized water as the buoyancy liquid. At least three bubble-free samples from each glass were characterized and those densities were used with the analyzed molar compositions to calculate the respective molar volumes.

Differential thermal analysis was performed either with a Perkin Elmer Differential Thermal Analyzer 7 using the Pyris Series - DTA 7 software or with a TA Instruments Q600 SDT using the TA Instrument Explorer software. 50mg samples ( $250\text{--}500\mu\text{m}$ ) were heated in a platinum crucible at a rate of  $10^\circ\text{C}/\text{min}$  to  $900^\circ\text{C}$  under a nitrogen atmosphere, and at least two tests were performed on each sample to verify

reproducibility.

Raman spectra were collected using a Horiba Jobin Yvon LabRAM ARAMIS micro-Raman spectrometer with a HeNe (632.8 nm) 17 mW laser or a diode (785 nm) 100 mW laser, depending on composition, and a 1200 grating at 10x magnification. Fluorescence in the spectra above  $1000\text{cm}^{-1}$  required the use of the diode source for the  $x = 30, 35, \text{ and } 40$  compositions in all three series. At least twenty 10 s scans were collected on each sample, and the respective average spectra are reported. For those spectra taken with the diode source, the Smooth (Adjacent-Averaging,  $\leq 25$  Points of Window) function of OriginPro (Massachusetts, USA), was used to reduce noise.

High pressure liquid chromatography (HPLC) was performed with a Dionex GP50-2 pump, an Ionpack AS7  $4 \times 250$  mm analytical ion exchange column, and an AD25 absorbance detector. Glass samples were ground to less than  $125\mu\text{m}$  particle size, dissolved overnight in a solution of 5 mM EDTA and 0.22 M NaCl (pH=10), and analyzed within 24 h. Three chromatographs were collected for each sample, using a linear solution gradient from 0.053 M NaCl to 0.5 M NaCl, both with 5 mM EDTA. The procedure was based on methods described by Sales *et al.* [30] to characterize the distributions of anion chain lengths in phosphate glasses.

Both  $^{11}\text{B}$  and  $^{31}\text{P}$  magic angle spinning nuclear magnetic resonance (MAS NMR) spectroscopy were performed using an Agilent DD2 spectrometer and Agilent 700/54 Premium Shielded superconducting magnet (16.4 T). Powdered glass was packed into a 3.2mm zirconia rotor and spun at a rate of 20 kHz. For the  $^{11}\text{B}$  measurements, at a resonance frequency of 224.52 MHz, the radio-frequency pulse lengths were 0.6  $\mu\text{s}$ , corresponding to a  $\pi/12$  tip angle, and a 5 s recycle delay occurred between acquisitions.  $^{11}\text{B}$  MAS NMR spectra were collected by signal averaging 160 to 2000 scans depending on boron content of the glass, and the data were processed without any additional line broadening (apodization) using commercial software.  $^{11}\text{B}$  MAS NMR spectra were referenced to a secondary shift standard of aqueous boric acid (19.6 ppm relative to  $\text{BF}_3$ -etherate). Spectra were fitted using DMfit Software [31], incorporating 2<sup>nd</sup>-order quadrupolar lineshapes for the trigonal boron resonances and a mixture of Gaussian and Lorentzian peaks for the tetrahedral boron resonances. A small correction to the  $\text{BO}_4$  peak intensity was made by fitting the first set of satellite transition spinning sidebands and incorporating a similar peak under the central transition resonances [32].

The radio-frequency pulse length for  $^{31}\text{P}$  experiments (283.27 MHz resonance frequency) was 1  $\mu\text{s}$ , corresponding to a  $\pi/6$  tip angle, and a 180 sec recycle delay was used between acquisitions.  $^{31}\text{P}$  MAS NMR spectra were collected by signal averaging of 54 to 400 scans, and the data were processed without any additional line broadening (apodization) using commercial software.  $^{31}\text{P}$  MAS NMR spectra were referenced to an 85%  $\text{H}_3\text{PO}_4$  solution at 0.0 ppm. All central peaks and their spinning sidebands were fitted with Gaussian lineshapes to determine peak areas.

## 3. Results

X-ray amorphous, visually homogeneous glasses were produced from melts from the  $16\text{Na}_2\text{O}-(24-y)\text{CaO}-y\text{SrO}-x\text{B}_2\text{O}_3-(60-x)\text{P}_2\text{O}_5$  series for all compositions in increments of  $10\text{B}_2\text{O}_3$  except at  $x = 50$ . For the  $y = 0$  series, several additional compositions were also produced and characterized, including ones to determine the crystallization range, which extended from  $x = 43$  to  $x = 56$ . The crystalline phases identified by XRD include a calcium borate phosphate phase ( $\text{Ca}_{9.93}(\text{P}_{5.84}\text{B}_{0.16}\text{O}_{24})$  ( $\text{B}_{0.67}\text{O}_{1.79}$ ), ICDD # 01-080-0537) at  $x = 43$  and a sodium calcium phosphate phase ( $\text{Na}_3\text{Ca}_6(\text{PO}_4)_5$ , ICDD # 00-011-0236) at  $x = 50$  and 56. The compositions analyzed by ICP-OES are shown in Table 3.1. There are minor, non-systematic deviations in the analyzed compositions ( $\pm 2.0$  mol %) from the as-batched compositions, including the crystallized samples. Throughout this paper, trends in structures and properties are reported in terms of the analyzed  $\text{B}_2\text{O}_3$  content (Table 1).

**Table 3.1**

As-batched and analyzed molar compositions for glasses in the series  $16\text{Na}_2\text{O}-(24-y)\text{CaO}-y\text{SrO}-x\text{B}_2\text{O}_3-(60-x)\text{P}_2\text{O}_5$ . ICP-OES analyses of glasses were done in triplicate and are reported as averages with one standard deviation. Asterisks indicate compositions that crystallized and were not measured in triplicate.

Sample		Analyzed by ICP-OES (mol %)				
<i>x</i>	<i>y</i>	$\text{Na}_2\text{O}$	$\text{CaO}$	$\text{SrO}$	$\text{B}_2\text{O}_3$	$\text{P}_2\text{O}_5$
0	0	14.2±0.1	25.5±0.1	–	0.0±0.3	60.4±0.5
10		13.9±0.1	25.3±0.1	–	10.8±0.1	50.0±0.2
20		13.7±0.1	25.0±0.2	–	20.3±0.1	41.0±0.3
23.3		12.8±0.2	24.4±0.3	–	23.7±0.3	39.0±0.1
30		13.9±0.1	24.5±0.3	–	30.0±0.4	31.6±0.2
35		13.0±0.1	24.4±0.1	–	35.9±0.5	26.7±0.3
40		14.1±0.1	24.2±0.2	–	40.6±0.2	21.2±0.1
43*		15.0	25.8	–	44.1	15.1
50*		14.9	25.3	–	52.3	7.5
56*		14.6	23.2	–	58.3	3.9
60		15.2±0.1	24.3±0.2	–	60.5±0.2	0.0±0.0
0	12	13.4±0.7	12.6±0.6	12.7±0.5	0.0±0.1	61.4±1.8
10		13.3±0.5	12.6±0.3	13.5±1.5	10.4±0.2	50.2±0.6
20		13.2±0.3	12.6±0.2	12.2±0.2	20.6±0.2	41.4±0.3
30		13.7±0.3	12.6±0.1	11.0±0.1	31.3±0.1	31.5±0.4
40		13.3±0.3	12.1±0.1	12.5±0.0	41.6±0.6	20.5±0.2
60		13.2±0.2	12.4±0.1	14.0±0.1	60.4±0.2	0.0±0.1
0	24	15.0±0.2	–	28.8±0.4	0.0±0.0	56.3±0.4
10		13.0±0.1	–	25.3±0.2	10.5±0.1	51.2±0.1
20		12.8±0.1	–	25.3±0.2	20.0±0.1	42.0±0.2
30		12.8±0.2	–	25.2±0.2	30.9±0.5	31.2±0.2
40		13.0±0.0	–	24.8±0.2	41.0±0.2	21.2±0.2
60		13.7±0.1	–	25.2±0.1	61.0±0.1	0.0±0.0

### 3.1. Raman spectroscopy

Fig. 3.1 shows representative Raman spectra collected from the SrO-free series ( $y = 0$ ) of the Na-(Ca,Sr)-borophosphate glasses; similar spectra were collected from the SrO-containing glasses and are shown in the appendix. It is worth noting that fluorescence in the spectra above  $1000\text{ cm}^{-1}$  required a change of excitation source for the  $x = 30, 35,$  and  $40$  compositions in all three series, as noted above. Table 3.2 lists the assignments for the dominant peaks, which fall into three general ranges: 1. Stretching modes for P-O nonbridging oxygens (NBO) are

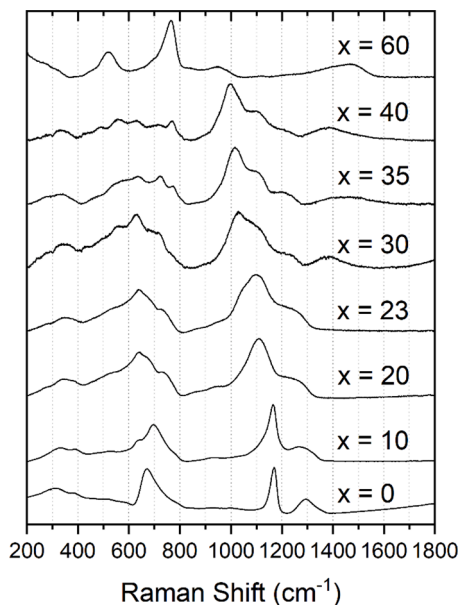


**Fig. 3.1.** Raman spectra from glasses in the SrO-free ( $y = 0$ ) nominal molar compositional series  $16\text{Na}_2\text{O}-24\text{CaO}-x\text{B}_2\text{O}_3-(60-x)\text{P}_2\text{O}_5$ . The intensity of each spectrum was normalized to the most intense peak in that spectrum for visual comparison.

**Table 3.2**

Assignments to the peaks in the Raman spectra collected from the  $16\text{Na}_2\text{O}-(24-y)\text{CaO}-y\text{SrO}-x\text{B}_2\text{O}_3-(60-x)\text{P}_2\text{O}_5$  glasses.

Raman Shift ( $\text{cm}^{-1}$ )	Assignment	Ref.
300	alkali/alkaline earth vibrational modes	[33]
520	B-O-B bending	[11,34–36]
550	P-O-P bending	[21,33]
630	P-O-B <sub>sym</sub> stretch, $P_{\text{JB}}^2$	[4,7,12,14,34]
700	P-O-P <sub>sym</sub> stretch, $P_{\text{OB}}^2$	[4,7,34]
720	six-membered borate ring with at least two $\text{BO}_4^-$ units	[4,12,37]
750, 770	P-O-B stretching modes	[34]
770	six-membered borate ring with at least one $\text{BO}_4^-$ unit	[4,12,21,34,37]
1160	$(\text{PO}_2)_{\text{sym}}$ stretch (NBO), $P_{\text{JB}}^2$ units	[4,7,12]
1050-1220	$(\text{PO}_3)_{\text{sym}}$ stretch, $P_{\text{JB}}^1$ units	[12,34,38]
1250	$(\text{PO}_2)_{\text{asym}}$ stretch (NBO), $P_{\text{JB}}^2$ units	[4,7,12]
1300	P=O <sub>sym</sub> stretch, $P_{\text{JB}}^3$ units	[4,7,12]
1300-1450	$\text{BO}_3$ in various borate rings	[34]
1450-1500	$\text{B}_{\text{JP}}^2$ vibrational modes	[4]

assigned to peaks in the  $1000-1300\text{ cm}^{-1}$  range, and nonbridging oxygens on B-triangles account for the broad peak near  $1400-1500\text{ cm}^{-1}$ ; 2. Stretching modes associated with bridging oxygens between phosphate and/or borate sites are assigned to peaks in the  $600-1000\text{ cm}^{-1}$  range; 3. Bending modes associated with P- and B-polyhedra, and vibrational modes associated with alkali and alkaline earth ions, are assigned to peaks below about  $500\text{ cm}^{-1}$ .

The spectrum from the borate-free ( $x = 0$ ) glass is similar to that reported for other ultraphosphate glasses with similar O/P ratios [39]. The intense peak at  $1160\text{ cm}^{-1}$  is due to the symmetric stretching modes of nonbridging oxygens on  $\text{Q}^2$  phosphate tetrahedra, and the broader, asymmetric peak centered near  $1300\text{ cm}^{-1}$  is due to overlapping bands assigned to the asymmetric P-NBO stretching modes on  $\text{Q}^2$  tetrahedra and the symmetric stretching modes of terminal oxygens on  $\text{Q}^3$  tetrahedra. Here, the  $\text{Q}^1$  terminology is used to describe P-tetrahedra with “i” bridging oxygens [40]. The asymmetric peak centered near  $700\text{ cm}^{-1}$  is due to the symmetric stretching modes of bridging oxygens that link neighboring P-tetrahedra.

The Raman spectrum of the phosphate-free ( $x = 60$ ) glass is similar to those reported for other alkali-rich borate glasses [35,36]. The intense peak at  $770\text{ cm}^{-1}$  has been assigned to the symmetric breathing modes associated with six-membered rings (three borons and three bridging oxygens) that include one or two B-tetrahedra [35]. These rings have been associated with several different borate superstructural units, including pentaborates, tetraborates, and diborates. The lower intensity peak near  $520\text{ cm}^{-1}$  has been assigned to the vibrational modes of B-tetrahedra that are not associated with one of the ring units [11, 34–36]. The broad peak that extends from about  $1300$  to  $1550\text{ cm}^{-1}$  has been assigned to the vibrational modes associated with nonbridging oxygens on trigonal borate sites [11,34–36].

There are systematic changes in the Raman spectra as borate replaces phosphate in the glass composition. With the initial addition of borate ( $x=10$ ), new peaks appear at  $630\text{ cm}^{-1}$ ,  $750\text{ cm}^{-1}$ , and  $770\text{ cm}^{-1}$  and steadily increase in relative intensity with increasing borate content. All three of these peaks have been assigned to vibrational modes associated with various borophosphate linkages [4,7,12,34]. The peak at  $720\text{ cm}^{-1}$  in the spectrum of the  $x = 35$  glass is assigned to a six membered borate ring, similar to what is found in the phosphate-free composition [4,7,12, 34]. The shift in the frequency of this peak to  $770\text{ cm}^{-1}$  with increasing borate content may indicate that the dominant borate ring changes from one with one trigonal borate unit to one with two trigonal borate units [4,12,21,34,37].

The transition from a phosphate to a borophosphate to a distinctly

borate network with increasing borate content is also reflected in the evolution of the Raman peaks in the 1000-1300  $\text{cm}^{-1}$  range. For example, the peak at 1160  $\text{cm}^{-1}$ , associated with the P-NBO stretching modes on  $Q^2$  tetrahedra, decreases in frequency and broadens with increasing borate contents. Both trends indicate that one or both of the bridging P-O-P bonds on those  $Q^2$  tetrahedra are being replaced either by a bridging oxygen to a borate site or by another nonbridging oxygen [11,34,38]. The spectra of glasses with  $B_2O_3$  contents from 23 to 40 mole % have three distinct peaks centered roughly around 1000, 1100, and 1200  $\text{cm}^{-1}$ , with the intensity of the 1000  $\text{cm}^{-1}$  peak becoming dominant in the borate-rich glass. Ducel *et al.* [31] explained similar compositionally-dependent changes in Raman spectra by the formation of isolated phosphate tetrahedra, ones that link to no other phosphate tetrahedra, in the structures of their borophosphate glasses.

Broad bands centered near 1400  $\text{cm}^{-1}$  appear in the spectra from glasses with  $x > 30$ , indicating the presence of trigonal borate species in the glass structure. Some of these triangles may be associated with borate rings that produce the sharp peaks in the 600-1000  $\text{cm}^{-1}$  range of spectra from the same glasses [29-30]. The spectra of the borophosphate glasses in this frequency range are much more complex than either the borate-free or phosphate free end members, indicating structures with a variety of phosphate, borophosphate, and borate linkages. With increasing borate content, the broad band around 1400  $\text{cm}^{-1}$  shifts to a higher frequency, around 1450  $\text{cm}^{-1}$ , indicating the presence of  $B^2$  species in the borate compositions.

### 3.2. High pressure liquid chromatography

Fig. 3.2 shows examples of chromatographs collected from the Na-(Ca,Sr)-borophosphate glasses. Peaks in the chromatographs with increasing retention time represent phosphate anions with increasing numbers of phosphate tetrahedra. For example, peaks near three minutes represent isolated, monophosphate anions ( $PO_4^{3-}$ ), those near seven minutes represent diphosphate anions ( $P_2O_7^{4-}$ ), those near ten minutes represent triphosphate anions ( $P_3O_{10}^{5-}$ ), etc. A peak labeled 3m,

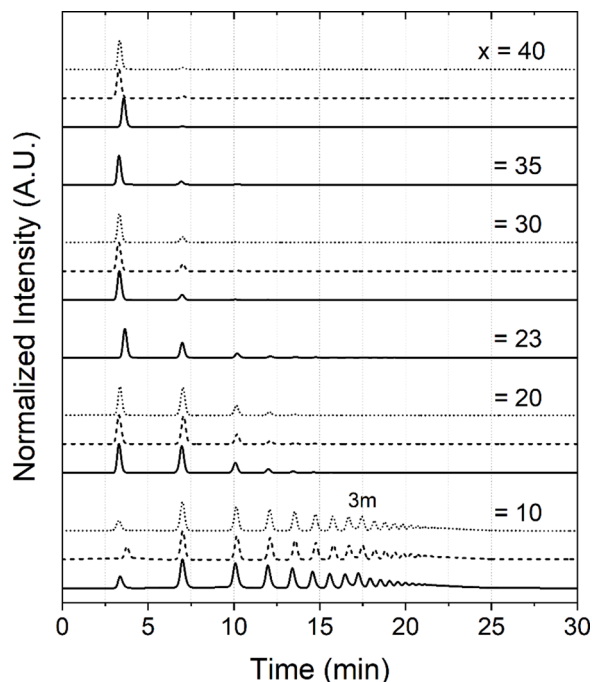


Fig. 3.2. Representative HPLC chromatographs from glasses with the nominal molar composition  $16Na_2O-(24-y)CaO-ySrO-xB_2O_3-(60-x)P_2O_5$ , where  $y = 0$  (solid),  $y = 12$  (dashed), and  $y = 24$  (dotted). The intensity of each chromatograph is normalized to the most intense peak in that chromatograph for visual comparison.

near 17 minutes, is assigned to a three-membered ring anion ( $P_3O_9^{3-}$ ) [41]. The chromatographs collected from the  $x = 0$  glasses are not shown here because the networks of those ultraphosphate compositions are partially hydrolyzed during the preparation of the chromatographic solutions [30,42] and so the resulting anion distributions are not representative of the original glass structure.

With the replacement of phosphate by borate, the dominant phosphate anions become increasingly smaller, until for the  $x = 40$  composition, only isolated monophosphate anions remain. The replacement of CaO for SrO has no obvious effect on the phosphate anion distributions.

### 3.3. Nuclear magnetic resonance spectroscopy

Fig. 3.3A shows representative  $^{11}B$  MAS NMR spectra collected from the borate-containing glasses. Based on previous NMR studies of borophosphate glasses [11,12,14,43], the peaks in the range 0 to -4 ppm are assigned to tetrahedral borate species, and the broader peak centered around approximately 15 ppm and exhibiting significant 2<sup>nd</sup>-order quadrupolar line broadening, is assigned to trigonal borate species. With increasing borate content, the tetrahedral peaks split to reveal new peaks at lower frequencies and a systematic decrease in the overall peak frequency. The broad trigonal peak is first detected in the spectrum of the  $x = 23$  glass, then increases in relative intensity for glasses with greater borate contents. There are no significant differences in the spectra from the CaO-, CaO/SrO-, and SrO-glasses, in contrast to another study which showed that SrO-containing borophosphate glasses have greater relative concentrations of tetrahedral borate sites than do CaO-containing glasses [27].

Fig. 3.3B shows representative  $^{31}P$  MAS NMR spectra. Two peaks are apparent in the spectra collected from the three borate-free glasses. The peaks near -28 ppm are assigned to the  $Q^2$  tetrahedra and the lower intensity peaks near -45 ppm are assigned to the  $Q^3$  tetrahedra that constitute the structures of these ultraphosphate glasses [44]. With the addition of borate to each series, the  $^{31}P$  MAS NMR peaks become broader and shift towards lower frequencies, trends seen in the NMR spectra of other borophosphate glasses [4,45].

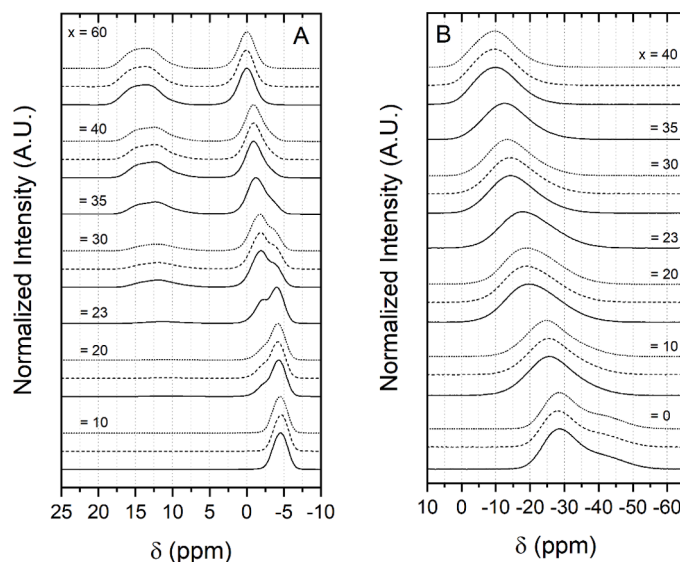


Fig. 3.3. The  $^{11}B$  MAS NMR (A) and  $^{31}P$  MAS NMR (B) spectra from glasses with the nominal molar composition  $16Na_2O-(24-y)CaO-ySrO-xB_2O_3-(60-x)P_2O_5$ , where  $y = 0$  (solid),  $y = 12$  (dashed), and  $y = 24$  (dotted). The intensity of each spectrum was normalized to the most intense peak in that spectrum for visual comparison.

### 3.4. Glass properties

The compositional dependences of density ( $\rho$ ) are shown in Fig. 3.4A. Density increases in the series  $\text{CaO} < (\text{CaO} + \text{SrO}) < \text{SrO}$ , a consequence of the greater average molar weight of the alkaline earth modifier. Density also goes through a maximum with increasing borate content for each series, near a  $\text{B}_2\text{O}_3$  content of 23 mole%.

Molar volume ( $V_m$ ) was calculated from density and the analyzed molar weight of the glass, then normalized to the analyzed atom fraction of oxygen [O] using Eq. (3.1):

$$V_m^o = \frac{MW_{\text{glass}}}{\rho \cdot [\text{O}]} \quad (3.1)$$

Fig. 3.4B shows the effects of composition on the normalized molar volumes. In general, the molar volumes of the SrO-glasses are 1-2% greater than those of the respective CaO-glasses, consistent with the larger size of the  $\text{Sr}^{2+}$  ion, but the type of alkaline earth has a much smaller effect on  $V_m^o$  than does the replacement of  $\text{P}_2\text{O}_5$  by  $\text{B}_2\text{O}_3$ . The break in the molar volume trend near  $x = 23$  indicates some change in the way that the ions pack in the borate-rich glasses.

The glass transition temperatures ( $T_g$ ) for all three series of glasses are shown in Fig. 3.5. The initial addition of borate to the phosphate base glass, up to  $x \sim 23$ , increases  $T_g$ , whereas further additions of borate have less effect. There appears to be no systematic effect of changing the alkaline earth modifier from CaO to SrO on  $T_g$ .

## 4. Discussion

The following nomenclature will be used to designate the P- and B-sites that constitute the glass structural networks. Phosphate sites are labeled as  $P_{jB}^i$ , where the superscript “i” is the total number of bridging oxygens on a phosphate tetrahedron and the subscript “j” is the number of oxygens on that same phosphate tetrahedron that bridge to a borate anion. Similarly, the borate sites that constitute the glass network are labeled as  $B_{jP}^i$ , where the superscript “i” is the total number of bridging oxygens on a borate polyhedron (tetrahedron or triangle) and the subscript “j” is the number of oxygens on that same borate polyhedron that bridge to a phosphate anion. For example, the quartz-like structure of  $\text{BPO}_4$  is made up of linkages between  $P_{4B}^4$  and  $B_{4P}^4$  tetrahedra. A metaphosphate glass will have a network based on  $P_{0B}^2$  tetrahedra [40] and a diborate glass will be constituted from  $B_{0P}^4$  and  $B_{0P}^3$  polyhedra [16, 36]. A borate triangle that has one nonbridging oxygen and two bridging oxygens to other borate polyhedra is designated  $B_{0P}^2$ .

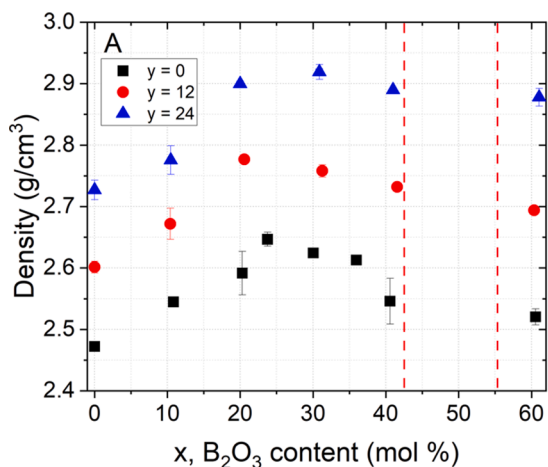


Fig. 3.4. The effects of analyzed borate contents on the density (A) and molar volume normalized to oxygen content (B) of glasses with the nominal molar composition  $16\text{Na}_2\text{O}-(24-y)\text{CaO}-y\text{SrO}-x\text{B}_2\text{O}_3-(60-x)\text{P}_2\text{O}_5$ . The dotted vertical lines mark the range of compositions in the  $y = 0$  series ( $43 \leq x \leq 56$ ) that crystallized upon quenching. Error bars represent one standard deviation and may be smaller than the symbol.

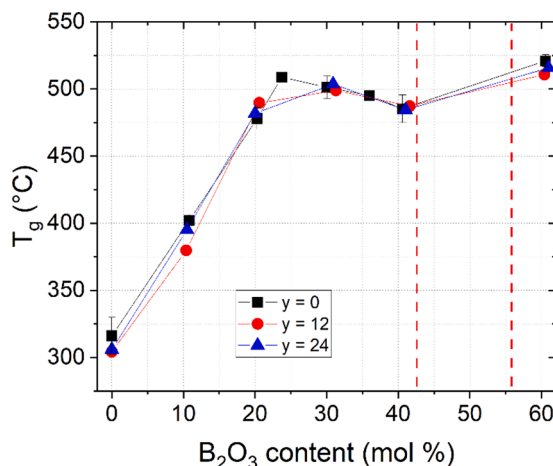
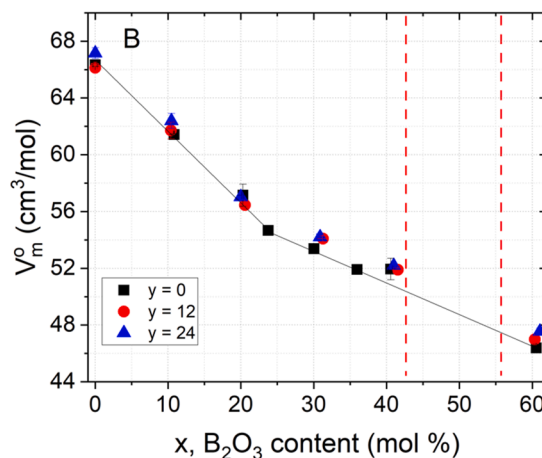


Fig. 3.5. The effects of analyzed borate contents on the glass transition temperatures for the glasses with the nominal molar composition  $16\text{Na}_2\text{O}-(24-y)\text{CaO}-y\text{SrO}-x\text{B}_2\text{O}_3-(60-x)\text{P}_2\text{O}_5$ . The dotted vertical lines mark the range of compositions in the  $y = 0$  series that crystallized upon quenching.

### 4.1. Quantitative mas NMR analysis

Representative fitted  $^{11}\text{B}$  MAS NMR and  $^{31}\text{P}$  MAS NMR spectra are shown in Fig. 4.1A and B, respectively. Two peaks were used to fit the  $^{11}\text{B}$  MAS NMR spectral envelope assigned to trigonal borate, one for neutral  $B_{0P}^3$  sites and a second for anionic  $B_{0P}^2$ ; the latter was identified by its relatively large electric field gradient asymmetry parameter ( $\eta_Q > 0.5$ ), following the methods reported by Rinke and Eckert [11]. For the current fits,  $\eta_Q$  was fixed as 0.6 for these  $B_{0P}^2$  peaks. Charge balance calculations shown in the appendix further support the presence of these anionic  $B_{0P}^2$  units, but only for the borate ( $x = 60$ ) compositions. Additional spectroscopic evidence, aside from high frequency bands in the Raman spectra, is needed to confirm the presence of these anionic  $B^2$  units in the borophosphate compositions, and so in the present study the entire trigonal boron signal is assigned to  $B_{0P}^3$  sites for  $x = 30, 35$ , and 40.

The tetrahedral boron satellite transition spinning sidebands under the central peak were accounted for by subtracting the average of the  $\pm 1$  sideband integrated intensities from the total integrated intensity of the tetrahedral peaks to obtain an accurate measure of the tetrahedral borate fraction. This part of the spectral envelope was then decomposed into Gaussian peaks representing different  $B_{jP}^i$  tetrahedra. The peak



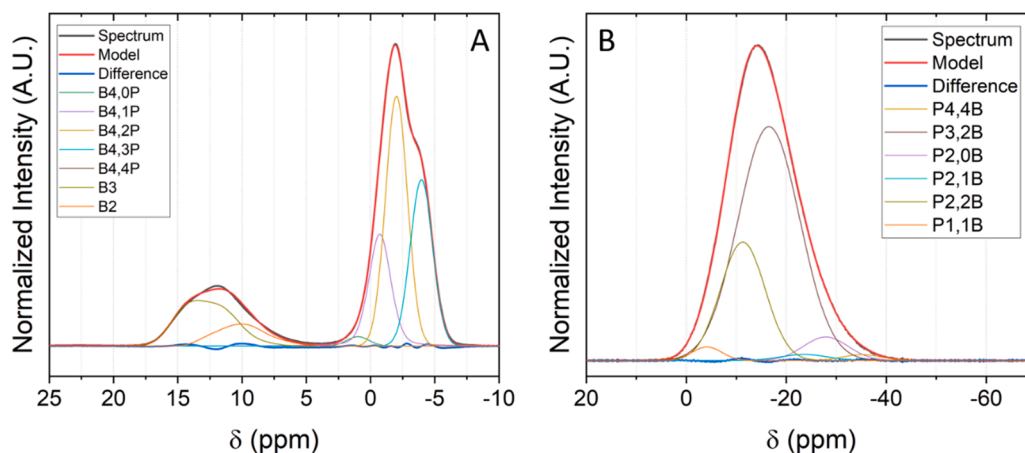


Fig. 4.1. Fitting the (A)  $^{11}\text{B}$  MAS NMR spectrum and the (B)  $^{31}\text{P}$  MAS NMR spectrum collected from the glass with the nominal molar composition  $16\text{Na}_2\text{O}-24\text{CaO}-30\text{B}_2\text{O}_3-30\text{P}_2\text{O}_5$ .

positions of the borate tetrahedra with respect to the borate content for all three series are summarized in Fig. 4.2. The shaded horizontal areas in Fig. 4.2 show the range of frequencies assigned to similar borate-species by Carta *et al.* [9]. There is good agreement for the assignments in the present study with those by Carta *et al.* [9] although they did not identify  $\text{B}_{0\text{P}}^4$  sites in their glasses.

The phosphate NMR spectra, an example of which is shown in Fig. 4.1B, were fit using Gaussian line-shapes and by constraining peak widths to 13–15 ppm for  $\text{P}_{\text{JB}}^3$  tetrahedra, 8–10 ppm for  $\text{P}_{\text{JB}}^2$  tetrahedra and 5–7 ppm for  $\text{P}_{\text{JB}}^1$  tetrahedra, following the methods of Carta *et al.* [9]. Similar  $\text{P}_{\text{JB}}^2$  and  $\text{P}_{\text{JB}}^3$  units have been assigned to the features of the  $^{31}\text{P}$  MAS NMR spectra collected from other alkali borophosphate glasses [4, 43]. Of note,  $\text{BPO}_4$  ( $\text{P}_{4\text{B}}^4$ ) units were identified in amounts less than 10% of the total phosphate sites for glasses with compositions in the range  $10 \leq x \leq 35$ , for all three series. The  $^{31}\text{P}$  NMR peak positions for each unit were averaged across each series ( $y = 0, 12$ , and  $24$ ) and are plotted in Fig. 4.3, along with the peak positions of relevant phosphate and borophosphate crystals, listed in Table 4.1. The shaded boxes represent the respective ranges of similar assignments made by Carta *et al.* [9].

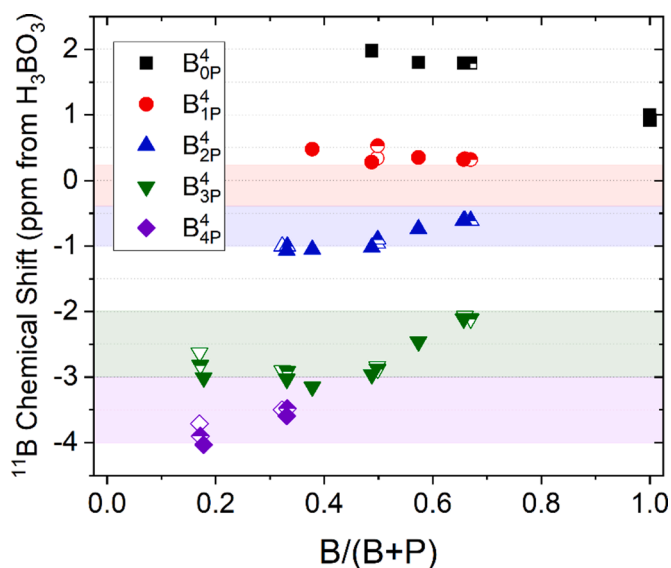


Fig. 4.2. The  $^{11}\text{B}$  peak positions of the borate tetrahedra in glasses with the nominal molar composition  $16\text{Na}_2\text{O}-(24-y)\text{CaO}-y\text{SrO}-x\text{B}_2\text{O}_3-(60-x)\text{P}_2\text{O}_5$ . The shaded boxes represent the respective ranges for each species, reported by Carta *et al.* [9].

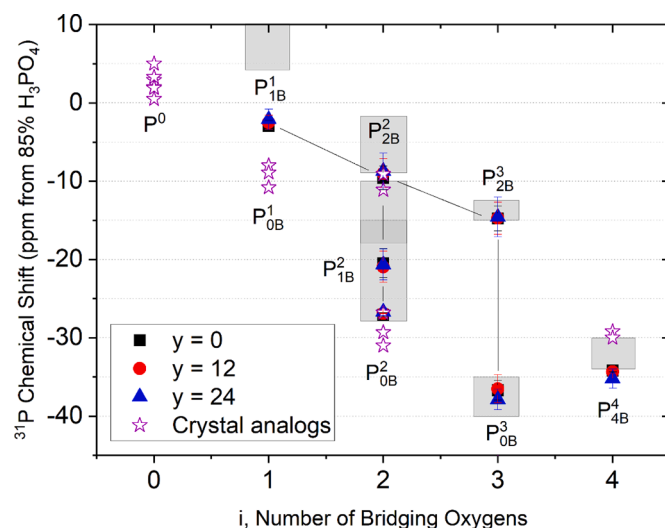


Fig. 4.3.  $^{31}\text{P}$  chemical shifts, averaged across each series, for the different phosphate tetrahedra identified in glasses with the nominal molar composition  $16\text{Na}_2\text{O}-(24-y)\text{CaO}-y\text{SrO}-x\text{B}_2\text{O}_3-(60-x)\text{P}_2\text{O}_5$ . The shaded boxes represent respective chemical shift ranges, reported by Carta *et al.* [9]. The chemical shifts reported for crystalline phosphates (Table 4.1) are shown as the open stars.

Table 4.1

The  $^{31}\text{P}$  MAS NMR peak shifts ( $\delta_{\text{iso}}$ ) reported for the indicated structural units in crystalline phosphates, used to compare with the respective peak assignments for the Na-Ca/Sr-borophosphate glasses in Fig. 4.3.

Structural Unit	Compound	$\delta_{\text{iso}}$ (ppm)	Reference
$\text{P}^0$	hydroxyapatite	2.9, 3.3	[46,47]
$\text{P}^0$	$\text{CaHPO}_4 \cdot 2\text{H}_2\text{O}$	2.0	[47]
$\text{P}^0$	$\beta\text{-Ca}_3(\text{PO}_4)_2$	0.5, 1.9, 5.0	[48]
$\text{P}_{1\text{OB}}^1$	$\alpha\text{-Ca}_2\text{P}_2\text{O}_7$	-8, -8.9, -10.8	[47,48]
$\text{P}_{2\text{OB}}^2$	$\beta\text{-Ca}(\text{PO}_3)_2$	-26.8, -29.3, -31.0	[47]
$\text{P}_{2\text{B}}^2$	$\text{CaBPO}_5$ , $\text{SrBPO}_5$	-9.1, -11.1	[49]
$\text{P}_{4\text{B}}^4$	$\text{BPO}_4$	-29.2, -30.0	[13,47,49]

Quantitative fits and peak assignments for the  $^{11}\text{B}$  MAS NMR and  $^{31}\text{P}$  MAS NMR spectra were made considering anion-to-cation charge balance, the structural information obtained by both Raman spectroscopy and HPLC, and the assignments made in other NMR studies of borophosphate glasses [11,12,43]. Notably,  $\text{P}_{2\text{B}}^3$  structures were assumed to

be the predominate moiety for  $P_{jB}^3$  units, and that  $P_{1B}^3$  and  $P_{3B}^3$  are not present, as noted by Raskar *et al.* [12]. Additionally, it was assumed that neutral  $B^3$  units would form before anionic trigonal species ( $B^2$ ). The relative fractions of borate and phosphate sites were determined using the analyzed compositions (Table 3.1) and the relative areas of the peaks in the fitted  $^{11}\text{B}$  and  $^{31}\text{P}$  MAS NMR spectra, and these are shown in Fig. 4.4A and B, respectively.  $B_{jP}^4$  units are the first borate sites to form with the initial replacement of  $\text{P}_2\text{O}_5$  by  $\text{B}_2\text{O}_3$  and their relative fractions reach a maximum in compositions with 20-30 mole %  $\text{B}_2\text{O}_3$ , the compositions at which borate triangles first appear. The relative fractions of these trigonal groups increase systematically with increasing  $\text{B}_2\text{O}_3$ -contents. At the same time, the fraction of  $P_{jB}^2$  units in the network decrease systematically with increasing  $\text{B}_2\text{O}_3$  content, whereas the fraction of the  $P_{jB}^3$  units remains relatively constant up to about 30 mole %  $\text{B}_2\text{O}_3$ . (As noted above, borate units systematically replace the phosphate units as next-nearest neighbors for these  $P_{jB}^3$  moieties with increasing  $\text{B}_2\text{O}_3$ -content.) Small fractions of  $P_{4B}^4$  are detected in the  $x = 10$  compositions, and small fractions of  $P_{jB}^1$  and  $P^0$  sites are present in the  $x = 40$  glasses.

Topological models of glass structures derived from constraint theories have proved useful for explaining composition-property trends for a variety of glass forming systems [28,50–53]. Hermansen assumed that borate was first incorporated into a phosphate network as  $B_{4P}^4$  units, and then beyond a critical B-to-P ratio, other anionic sites would emerge, in the order  $B_{jP}^4 > P_{jB}^2 > P_{jB}^1 > P^0 > B^2$  [14]. To simplify the calculations used for their model, Hermansen also assumed that no more than two different phosphate sites ( $P_{jB}^i$ ) would be present in a borophosphate network and that the anionic charges of the network sites are balanced by the modifying cation charges. Table 4.2 shows the equations used by Hermansen to describe the compositional dependences of B- and P-sites for glasses with the nominal molar compositions  $x\text{R}'\text{O}(1-x)[y\text{B}_2\text{O}_3(1-y)\text{P}_2\text{O}_5]$ , where  $\text{R}'\text{O}$  represents both alkali and alkaline earth oxides, and these equations are plotted as the solid lines in Fig. 4.4A and B [14].

In general, the compositional dependences of the relative concentrations of the major B- and P-sites derived from the  $^{11}\text{B}$  and  $^{31}\text{P}$  MAS NMR spectra of the glasses in the present study are consistent with the predictions of the Hermansen model. In particular, Hermansen predicted that only  $B_{jP}^4$  sites would be present in glasses with up to 23 mole %  $\text{B}_2\text{O}_3$  and indeed, significant concentrations of trigonal borate units were detected only in glasses with greater borate concentrations (Fig. 4.4A). Hermansen predicted similar breaks in the compositional dependences of the  $P_{jB}^3$  and  $P_{jB}^2$  unit concentrations at 23 mole %  $\text{B}_2\text{O}_3$ , although these changes are less obvious in the quantitative NMR data

shown in Fig. 4.4B. The disproportionation of  $P_{jB}^2$  sites to  $P_{jB}^3$  and  $P_{jB}^1$  sites has been noted in previous studies of borophosphate glasses modified with higher field strength cations, like  $\text{Ca}^{2+}$  [14,54], and similar reactions may account for some of the site-concentration differences between the present measurements and Hermansen's predictions.

There are several other differences between the quantitative site analyses of the glasses in the present study and those predicted by Hermansen. First, the  $^{31}\text{P}$  MAS NMR spectra in the present study (Fig. 3.3B) reveal small (<10 %) fractions of  $P_{4B}^4$  sites in glasses with up to 20 mole %  $\text{B}_2\text{O}_3$ ; Hermansen assumed that these sites would not form in these glasses. And secondly, the  $^{31}\text{P}$  MAS NMR spectra reveal that these borophosphate glasses have more than two distinct P-sites, an interpretation consistent with the complexity of the Raman spectra in the 1000-1300  $\text{cm}^{-1}$  range (Fig. 3.1) and with the large number of P-anions detected by HPLC for glasses with a  $\text{B}_2\text{O}_3$  content less than about 35 mole% (Fig. 3.2).

Despite these differences, the Hermansen model still provides useful insight into the evolution of the borophosphate network with increasing borate contents, insight that will be used below to explain the compositional dependence of the glass properties.

#### 4.2. Oxygen speciation

The equations in Table 4.3 summarize those used by Hermansen *et al.* to calculate oxygen speciation based on the borate and phosphate site concentration equations in Table 4.2. In these equations,  $b$  is a measure of the allowable  $\text{B}^4\text{-O-B}^4$  bonds per  $B_{jP}^4$  unit, and Hermansen *et al.* assumed that no tetrahedral borate units were connected to another tetrahedral boron ( $b = 0$ ).

In the present study, the number of bridging oxygens per glass former and non-bridging oxygens per glass former were calculated from the fractions of structural units,  $[B_{jP}^i]$  and  $[P_{jB}^i]$ , obtained by MAS NMR using Eqs. (4.4) and (4.5):

$$\frac{[\text{O}]}{(\text{B} + \text{P})} = \sum \left( \frac{i}{2} [B_{jP}^i] \right) + \sum \left( \frac{i}{2} [P_{jB}^i] \right) \quad (4.4)$$

$$\frac{[\text{NBO}]}{(\text{B} + \text{P})} = [B^2] + \sum \left( (4-i) [P_{jB}^i] \right) \quad (4.5)$$

In this analysis, the  $\text{B}^3$  units are assumed not to have bridging oxygens to phosphate tetrahedra. This assumption is consistent with REDOR experiments that could not confirm the presence of  $\text{P-O-B}^3$  bonds [11, 13], although such linkages have been identified in a  $^{11}\text{B}(^{31}\text{P})$  dipolar heteronuclear multiple quantum coherence study of alkali borophosphate glasses [66]. The fraction of each type of bridging oxygen to

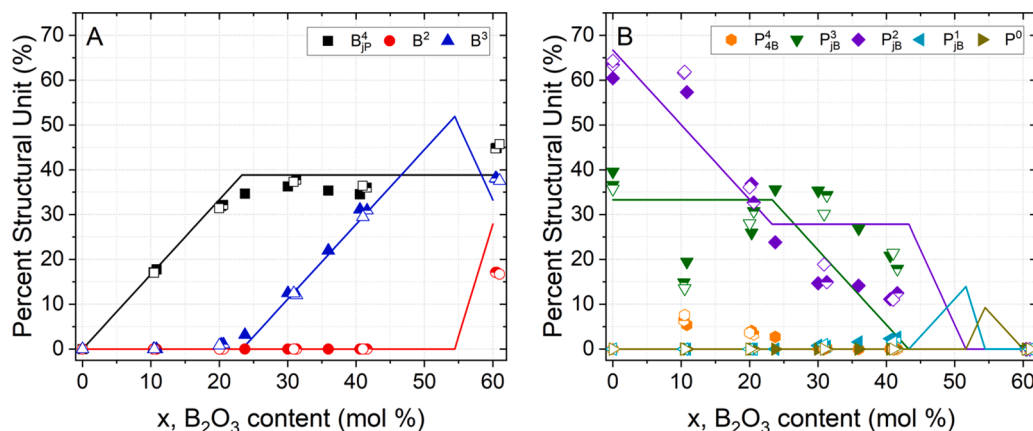


Fig. 4.4. The respective fractions of borate (A) and phosphate (B) sites obtained from the  $^{11}\text{B}$  and  $^{31}\text{P}$  MAS NMR spectra from glasses with the nominal molar composition  $16\text{Na}_2\text{O}-(24-y)\text{CaO}-y\text{SrO}-x\text{B}_2\text{O}_3-(60-x)\text{P}_2\text{O}_5$ , where  $y = 0$  (solid symbols), 12 (half-filled symbols) and 24 (open symbols). The solid lines are the predicted distributions from the model proposed by Hermansen *et al.* [14].

**Table 4.2**

Summary of the equations used by Hermansen to determine structural units for the glass compositions shown in Fig. 4.4 [14].

Structural Unit	Set of Equations
[B <sup>4</sup> ]	$\begin{cases} y, y \leq y^* \\ y^*, y^* < y \end{cases}$
[B <sup>3</sup> ]	$\begin{cases} y - [B^4], \frac{x}{1-x} \leq y^* + 3 \times (1-y) \\ y - [B^4] - \left(\frac{x}{1-x} - y^* - 3 \times (1-y)\right), y^* + 3 \times (1-y) < \frac{x}{1-x} \end{cases}$
[B <sup>2</sup> ]	$\begin{cases} 0, \frac{x}{1-x} \leq y^* + 3 \times (1-y) \\ \frac{x}{1-x} - y^* - 3 \times (1-y), y^* + 3 \times (1-y) < \frac{x}{1-x} \end{cases}$
[P <sup>3</sup> ]	$\begin{cases} (1-y) - \left(\frac{x}{1-x} - [B^4]\right), \frac{x}{1-x} \leq y^* + (1-y) \\ 0, y^* + (1-y) < \frac{x}{1-x} \end{cases}$
[P <sup>2</sup> ]	$\begin{cases} \frac{x}{1-x} - [B^4], \frac{x}{1-x} \leq y^* + (1-y) \\ 2 \times (1-y) - \left(\frac{x}{1-x} - [B^4]\right), y^* + (1-y) < \frac{x}{1-x} \leq y^* + 2 \times (1-y) \\ 0, y^* + 2 \times (1-y) < \frac{x}{1-x} \end{cases}$
[P <sup>1</sup> ]	$\begin{cases} 0, \frac{x}{1-x} \leq y^* + (1-y) \\ \left(\frac{x}{1-x} - [B^4]\right) - (1-y), y^* + (1-y) < \frac{x}{1-x} \leq y^* + 2 \times (1-y) \\ 3 \times (1-y) - \left(\frac{x}{1-x} - [B^4]\right), y^* + 2 \times (1-y) < \frac{x}{1-x} \leq y^* + 3 \times (1-y) \\ 0, y^* + 3 \times (1-y) < \frac{x}{1-x} \end{cases}$
[P <sup>0</sup> ]	$\begin{cases} 0, \frac{x}{1-x} \leq y^* + 2 \times (1-y) \\ \left(\frac{x}{1-x} - [B^4]\right) - 2 \times (1-y), y^* + 2 \times (1-y) < \frac{x}{1-x} \leq y^* + 3 \times (1-y) \\ (1-y), y^* + 3 \times (1-y) < \frac{x}{1-x} \end{cases}$

**Table 4.3**

Equations used by Hermansen *et al.* to determine oxygen speciation in borophosphate glasses with nominal compositions of xR'O(1 - x)[yB<sub>2</sub>O<sub>3</sub>(1 - y)P<sub>2</sub>O<sub>5</sub>] [14].

Oxygen Speciation	Set of Equations
[BØP]	$\begin{cases} \frac{(4-b) \times [B^4]}{(x + (1-x) \times (3y + 5(1-y)))/(2 \times (1-x))}, y \leq y^* \\ \frac{4 \times [P^4] + 3 \times [P^3] + 2 \times [P^2] + 1 \times [P^1]}{(x + (1-x) \times (3y + 5(1-y)))/(2 \times (1-x))}, y^* < y \end{cases}$
[BØB]	$=$
[PØP]	$\begin{cases} \frac{1}{2} \times \frac{(3 \times [B^3] + 2 \times [B^2] + 1 \times [B^1])}{(x + (1-x) \times (3y + 5(1-y)))/(2 \times (1-x))}, y \leq y^* \\ \frac{1}{2} \times \frac{(4 \times [B^4] + 3 \times [B^3] + 2 \times [B^2] + 1 \times [B^1])}{(x + (1-x) \times (3y + 5(1-y)))/(2 \times (1-x))} - \frac{1}{2} \times [BØP], y^* < y \end{cases}$
[NBO]	$=$ $\begin{cases} 0, y^* < y \\ \frac{1 \times [B^2] + 2 \times ([B^1] + [P^2]) + 3 \times ([B^0] + [P^1]) + 4 \times [P^0]}{(x + (1-x) \times (3y + 5(1-y)))/(2 \times (1-x))} \end{cases}$

the total number of oxygens was calculated from the fraction of structural units, [B<sup>i</sup><sub>jp</sub>] and [P<sup>i</sup><sub>jb</sub>], obtained by MAS NMR (summarized in Appendix), using Eqs. (4.6), (4.7) and (4.8):

$$[BØP] = \frac{\sum \left(\frac{i}{2} [B_{jp}^i]\right) + \sum \left(\frac{i}{2} [P_{jb}^i]\right)}{Ø + NBO} \tag{4.6}$$

$$[BØB] = \frac{\sum \left(\frac{(i-j)}{2} [B_{jp}^i]\right)}{Ø + NBO} \tag{4.7}$$

$$[PØP] = \frac{\sum \left(\frac{(i-j)}{2} [P_{jb}^i]\right)}{Ø + NBO} \tag{4.8}$$

The compositional dependences of the fractions of the three bridging oxygen species ([BØP], [BØB], and [PØP]), and non-bridging oxygens associated with borate and phosphate units ([NBO(B)] and [NBO(P)], respectively), are shown in Fig. 4.5. The solid lines are the trends predicted by the Hermansen model. The trends in speciation can be divided into two regions with x = 23 as the pivotal composition. It is worth noting that this composition is the same at which the structural model by Hermansen predicts the maximum fraction of tetrahedral borate units and the onset of the formation of trigonal borate units.

In the compositional range 0 ≤ x ≤ 23, an exchange of PØP for BØP linkages occurs as tetrahedral borate units replace phosphate units to form a borophosphate network. At the pivotal composition (x = 23), the maximum in [BØP] marks the point at which the glass structure is a fully interconnected borophosphate network. Above this composition (x > 23), the additional borate units are incorporated into a distinctly borate network as BØP linkages are replaced by BØB linkages, including those that link increasing fractions of trigonal borate sites (Fig. 4.4A).

The primary assumption made by Hermansen *et al.* that differs from the results of this analysis is that the borate units first form heteroatomic linkages with phosphate units before they form homoatomic linkages to other borate units. There is clear evidence in the <sup>11</sup>B MAS NMR spectra for a greater fraction of homoatomic BØB bonds in the structures of glasses in the compositional range 20 ≤ B<sub>2</sub>O<sub>3</sub> ≤ 40 (mol %), and in the <sup>31</sup>P MAS NMR spectra and the chromatographs for the presence for

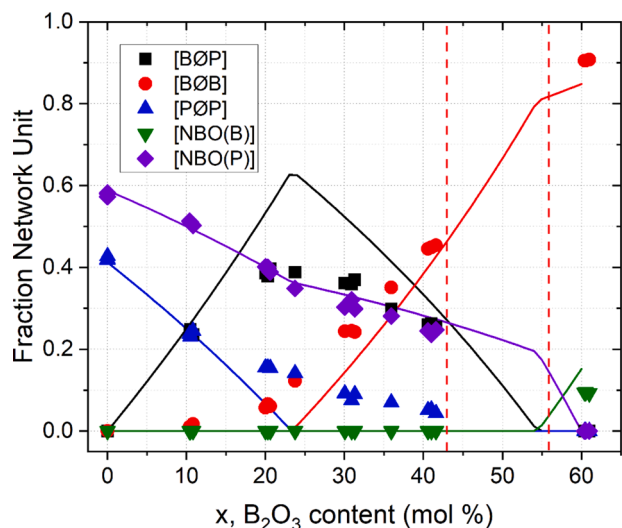


Fig. 4.5. Compositional dependence of the oxygen speciation for glasses with the nominal molar composition  $16\text{Na}_2\text{O}-(24-y)\text{CaO}-y\text{SrO}-x\text{B}_2\text{O}_3-(60-x)\text{P}_2\text{O}_5$ , where  $y=0$ ,  $y=12$ , and  $y=24$ . Solid lines are the predictions from Hermansen's structural model. The dotted lines mark the range where the compositions crystallize upon quenching.

greater fractions of homoatomic PØP linkages in in the same glasses leading to smaller fractions of heteroatomic BØP than are predicted by Hermansen's structural model. There is good agreement between the compositional dependences of the nonbridging oxygens fractions, ([NBO (B)] and [NBO(P)], and Hermansen's predictions.

Fig. 4.6 plots the compositional dependence of the number of bridging oxygens per glass former for the three series of CaO/SrO borophosphate glasses. This metric will be used below to explain the compositional dependence of the glass transition temperatures.

The Raman spectra in Fig. 3.1 show an evolution in the network structures of these glasses from phosphate to borophosphate to borate as  $\text{B}_2\text{O}_3$  replaces  $\text{P}_2\text{O}_5$ , consistent with the interpretations of the MAS NMR and HPLC data. The intense peak centered near  $1160\text{ cm}^{-1}$  in the spectrum of the borate-free compositions broadens and shifts to lower frequencies with increasing  $\text{B}_2\text{O}_3$  content. This peak is assigned to the symmetric stretching modes of nonbridging oxygens on  $\text{Q}^2$  phosphate tetrahedra, and the shift to lower frequencies is an indication of the replacement of a phosphate by a borate as the next nearest neighbors;

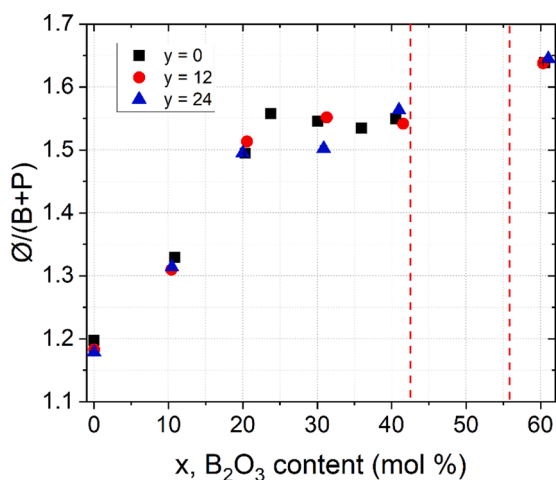


Fig. 4.6. Compositional dependence of the number of bridging oxygens per glass former ( $\text{Ø}/(\text{B}+\text{P})$ ) for glasses with the nominal molar composition  $16\text{Na}_2\text{O}-(24-y)\text{CaO}-y\text{SrO}-x\text{B}_2\text{O}_3-(60-x)\text{P}_2\text{O}_5$ . The vertical dotted lines mark the range where the compositions crystallize upon quenching.

viz., the conversion of  $\text{P}_{0\text{B}}^2$  to  $\text{P}_{1\text{B}}^2$  [4,14]. The development of these PØB linkages is further indicated by the increase in the intensity of the Raman peak at  $1050\text{ cm}^{-1}$  with increasing borate content. The relative intensity of this peak is maximized for the glass where  $x = 30$ . In the Raman spectra from the high-borate compositions, where  $x > 35$ , peaks near  $720$  and  $750\text{ cm}^{-1}$  assigned to borate vibrational modes become apparent. These features are consistent with the appearance of the trigonal borate sites in the  $^{11}\text{B}$  MAS NMR spectra (Fig. 3.3).

#### 4.3. Phosphate anion distributions

When phosphate glasses are dissolved under the conditions used to prepare the HPLC solutions, ionic bonds that link the phosphate anions through the modifying cations are hydrated, releasing those anions to be separated by the chromatography column and then analyzed. The hydrolysis of the bridging oxygen bonds (PØP) that link the neighboring P-tetrahedra that constitute those anions is relatively slow and so the distribution of anions recorded by HPLC is assumed to represent that found in the original glass [30]. However, when ultraphosphate glasses react in aqueous solutions, the  $\text{P}_{0\text{B}}^3$  units hydrolyze to release smaller P-anions and so the distributions of those anions in solution are different from those in the original glass [42,55,56]. Therefore, quantitative structural information for phosphate glasses from HPLC is limited to the polyphosphate ( $\text{O}/\text{P} > 3$ ) compositions [57–60].

In the preparation of the HPLC samples from the borophosphate glasses in the present study, the oxygens that bridge borate and phosphate units (BØP) are assumed to hydrolyze much faster than the bridging PØP bonds. Protonated tetrahedral borates which initially form when borates are hydrated are unstable and immediately convert to more stable protonated trigonal borates [61,62], leading to the hydrolysis of the bridging BØB bonds and the release of borate species to solution [63]. Similar reactions are assumed to occur with the borophosphate bonds, leading to the separate release of phosphate anions and boric acid.

Fig. 4.7 compares the quantitative P-speciation results from the HPLC data with those from the  $^{31}\text{P}$  MAS NMR spectra. Here, the different  $\text{P}_{j\text{B}}^i$  units identified in the NMR spectra are combined to their respective values of "i" and compared to the fractions of  $\text{P}^i$  sites obtained directly from the associated chromatographs. In this analysis, it was assumed that every  $\text{P}_{2\text{B}}^3$  unit identified in the NMR data was hydrolyzed to form a  $\text{P}^0$  anion in the HPLC solutions, leading to reasonably good agreement

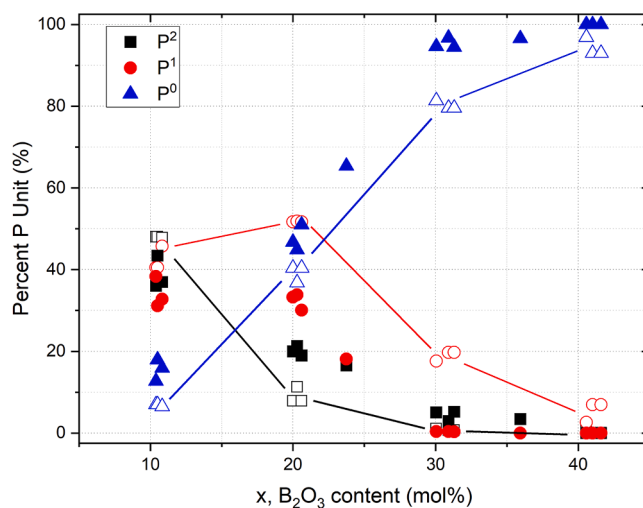


Fig. 4.7. Fractions of  $\text{P}^0$ ,  $\text{P}^1$ , and  $\text{P}^2$  units for glasses with the nominal molar composition  $16\text{Na}_2\text{O}-(24-y)\text{CaO}-y\text{SrO}-x\text{B}_2\text{O}_3-(60-x)\text{P}_2\text{O}_5$  as measured by  $^{31}\text{P}$  MAS NMR (closed symbols) and HPLC (open symbols). The lines are meant as guides for the eye.

between the two data sets .

The average P-anion size ( $\bar{n}$ ) in a polyphosphate glass can be predicted from its composition using Eq. (4.4) [40,64]:

$$\bar{n} = \frac{1}{([\text{O}]/[\text{P}]) - 3} \quad (4.1)$$

Here, it is assumed that all oxygens in the glass structure are linked to a phosphate unit. In the present borophosphate glasses, some fraction of oxygens bridge neighboring borate units as BØB bonds and so do not modify the phosphate linkages. However, if these oxygens are subtracted from the total oxygen content, then, as shown in Fig. 4.8, the average P-anion size measured by NMR is in good agreement with that predicted by the following modified version of Eq. (4.4):

$$\bar{n}_{mod} = \frac{1}{([\text{O}_{tot} - \text{O}_{BØB}]/[\text{P}]) - 3} \quad (4.2)$$

#### 4.4. Glass properties

Topological structural models, like the one proposed by Hermansen, et al. for borophosphate glasses, have proved to be useful for predicting properties that are sensitive to the nature of the glass-forming network [14]. In the present study, the similarity in the compositional dependence of the glass transition temperature (Fig. 3.5) and the number of bridging oxygens per glass-forming cation (Fig. 4.6) indicates that the former directly depends on the latter. Indeed, Fig. 4.9 shows a systematic increase in  $T_g$  with increasing numbers of Ø/(B+P). Rinke et al. observed a similar correlation between glass transformation temperatures and the network former connectivity for Na-borophosphate glasses [11].

The dependence of  $T_g$  on average number of network crosslinks shown in Fig. 4.9 can be used to explain the compositional dependence of  $T_g$  (Fig. 3.5) and to highlight the significance of the glasses with 23 mole %  $\text{B}_2\text{O}_3$ . The initial replacement of  $\text{P}_2\text{O}_5$  by  $\text{B}_2\text{O}_3$  creates highly cross-linked  $B_{4p}^+$  network sites that replace less-crosslinked  $P_{0b}^3$  and  $P_{0b}^2$  units that constitute the structure of the ultraphosphate ( $x = 0$ ) glasses. Indeed, the average Ø/(B+P) ratio increases from 1.22 to 1.55 when the  $\text{B}_2\text{O}_3$  content increases from 0 to 23 mole %. Further replacement of  $\text{P}_2\text{O}_5$  by  $\text{B}_2\text{O}_3$  ( $23 \leq x \leq 40$ ) creates lower dimensional trigonal borates and depolymerized phosphate sites, causing  $T_g$  to decrease. The

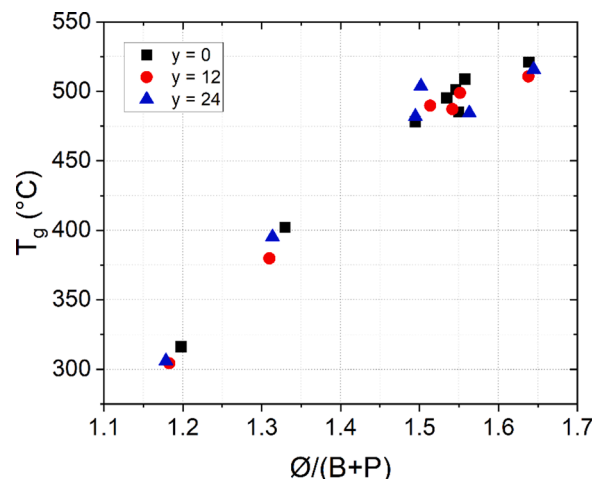


Fig. 4.9. The dependence of glass transition temperature on the number of bridging oxygens per glass former (Ø/(B+P)) for glasses with the nominal molar composition  $16\text{Na}_2\text{O}-(24-y)\text{CaO}-y\text{SrO}-x\text{B}_2\text{O}_3-(60-x)\text{P}_2\text{O}_5$ .

phosphate-free compositions ( $x = 60$ ) have the highest glass transition temperatures and the greatest Ø/(B+P) ratios. This analysis indicates that the type of bridging oxygen bond (PØP, BØP, BØB) has less influence on the glass transition temperature than the total number of bridging oxygens per network former.

The effects of composition on molar volume (Fig. 3.4B) are more subtle, but the break in the trend near 23 mole %  $\text{B}_2\text{O}_3$  can also be explained by the transition in the structural motif at this composition. The initial replacement of  $\text{P}_2\text{O}_5$  by  $\text{B}_2\text{O}_3$  results in the replacement of PØP bonds by BØP bonds, with the relative fraction of the latter reaching a maximum at 23 mole%  $\text{B}_2\text{O}_3$  (Fig. 4.5). Above this composition, BØB bonds become increasingly dominant in the glass structures. Qiu et al. studied the structures of Na-borophosphate glasses using high-energy X-ray diffraction and found that the distances between network formers across bridging oxygens decreased in the order PØP ( $2.88\text{Å}$ ) > BØP ( $2.73\text{Å}$ ) > BØB ( $2.63\text{Å}$ ) [65]. The trend towards shorter average bond distances is consistent with the overall decrease in  $V_m^0$  with increasing  $\text{B}_2\text{O}_3$  content (Fig. 3.4B), and the steeper slope in the  $V_m^0$  trend below 23 mole% is consistent with the greater difference between the PØP and BØP bond distances. At compositions above  $x > 23$ , BØP linkages are exchanging for BØB linkages, which are closer in bond length, leading to a less negative change in molar volume per oxygen.

#### 5. Summary

Borate and phosphate site speciation in the structures of three series of glasses with the nominal molar composition  $16\text{Na}_2\text{O}-(24-y)\text{CaO}-y\text{SrO}-x\text{B}_2\text{O}_3-(60-x)\text{P}_2\text{O}_5$  (mol%), where  $0 \leq x \leq 60$  and  $y = 0, 12, \text{ and } 24$ , were quantified by  $^{11}\text{B}$  and  $^{31}\text{P}$  MAS NMR and found to be in good agreement with the structural information obtained by HPLC and Raman spectroscopy. The initial addition of  $\text{B}_2\text{O}_3$  creates tetrahedral borophosphate units ( $B_{4p}^+$ ) that reduce the average size of the P-anions that constitute the glass structures. Trigonal borates are present in glasses with greater  $\text{B}_2\text{O}_3$  contents, and become more significant as the overall compositions and structures evolve from borophosphates to borates.

The evolution of these structures is in general agreement with the topological model proposed by Hermansen, et al., and indicate that a local maximum in network cross-link density is reached at 23 mole %  $\text{B}_2\text{O}_3$ , where a maximum in the fraction of BØP bonds is expected. Above this composition BØB bonds associated with tetrahedral and trigonal B-sites become dominant. Changes in the compositional dependences of the glass transition temperature and the molar volume occur at 23 mole

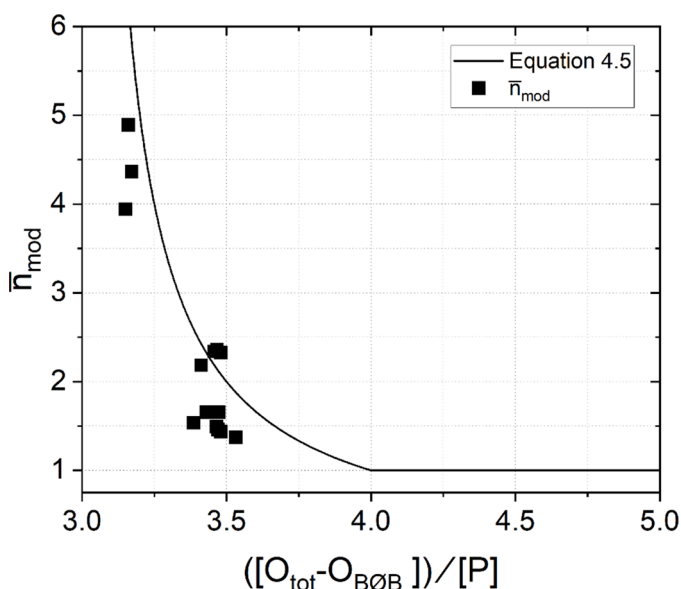


Fig. 4.8. Average phosphate chain length determined by  $^{31}\text{P}$  MAS NMR ( $\bar{n}_{mod}$ ) compared to what is expected from the modified O/P ratio ( $[\text{O}_{tot}-\text{O}_{BØB}]/[\text{P}]$ ), which excludes oxygens sequestered in BØB linkages.

% B<sub>2</sub>O<sub>3</sub>, and are consistent with the changes in the molecular-level structures of these glasses.

### CRedit authorship contribution statement

**Parker T. Freudenberger:** Conceptualization, Methodology, Investigation, Validation, Formal analysis, Writing – original draft, Writing – review & editing, Visualization. **Rebekah L. Blatt:** Investigation, Validation, Formal analysis, Writing – review & editing. **Randall E. Youngman:** Investigation, Validation, Formal analysis, Writing – review & editing. **Richard K. Brow:** Conceptualization, Writing – original draft, Writing – review & editing, Visualization, Supervision, Funding acquisition.

### Declaration of Competing Interest

The authors declare that they have no known competing financial interests or personal relationships that could have appeared to influence the work reported in this paper.

### Data Availability

Data will be made available on request.

### Acknowledgements

This work was supported by the Graduate Assistance in Areas of National Need (GAANN) fellowship from the US Department of Education. The authors would like to thank Alana Buznego for her assistance with glass preparation and Dr. Eric Bohannon for his assistance with the X-ray diffraction analyses.

### Supplementary materials

Supplementary material associated with this article can be found, in the online version, at doi:10.1016/j.jnoncrysol.2022.121966.

### References

- [1] JW Lim, ML Schmitt, RK Brow, SW. Yung, Properties and structures of tin borophosphate glasses, *J. NonCryst. Solids* 356 (28–30) (2010) 1379–1384, <https://doi.org/10.1016/j.jnoncrysol.2010.02.019>.
- [2] J Massera, I Ahmed, L Petit, V Aallos, L. Hupa, Phosphate-based glass fiber vs. bulk glass: change in fiber optical response to probe in vitro glass reactivity, *Mater. Sci. Eng.* 37 (2014) 251–257, <https://doi.org/10.1016/j.msec.2014.01.021>.
- [3] J Massera, Y Shpotyuk, F Sabatier, et al., Processing and characterization of novel borophosphate glasses and fibers for medical applications, *J. NonCryst. Solids* 425 (2015) 52–60, <https://doi.org/10.1016/j.jnoncrysol.2015.05.028>.
- [4] R Christensen, G Olson, SW. Martin, Structural Studies of Mixed Glass Former 0.35Na<sub>2</sub>O+0.65[xB<sub>2</sub>O<sub>3</sub>+(1-x)P<sub>2</sub>O<sub>5</sub>] Glasses by Raman and <sup>11</sup>B and <sup>31</sup>P magic angle spinning nuclear magnetic resonance spectroscopies, *J. Phys. Chem. B* 117 (7) (2013) 2169–2179, <https://doi.org/10.1021/jp308494a>.
- [5] N Sharmin, J Parsonsa, CD Rudd, I Ahmed, Effect of boron oxide addition on fibre drawing, mechanical properties and dissolution behaviour of phosphate-based glass fibres with fixed 40, 45 and 50 mol% P<sub>2</sub>O<sub>5</sub>, *J. Biomater. Appl.* 29 (5) (2014) 639–653, <https://doi.org/10.1177/0885328214539824>.
- [6] Takebe H, Suzuki Y, Uemura T. Effect of B<sub>2</sub>O<sub>3</sub> and Al<sub>2</sub>O<sub>3</sub> additions on the structure of phosphate glasses. 2014;55(5):207–210. doi:10.1115/1.4024145.
- [7] IJ Hidi, G Melinte, R Stefan, M Bindea, L. Baia, The study of the structure and bioactivity of the B<sub>2</sub>O<sub>3</sub> • Na<sub>2</sub>O • P<sub>2</sub>O<sub>5</sub> system, *J. Raman Spectrosc.* 44 (8) (2013) 1187–1194, <https://doi.org/10.1002/jrs.4330>.
- [8] N Sharmin, MS Hasan, AJ Parsons, et al., Effect of boron addition on the thermal, degradation, and cytocompatibility properties of phosphate-based glasses, *Biomed. Res. Int.* 2013 (2013), <https://doi.org/10.1155/2013/902427>.
- [9] D Carta, D Qiu, P Guerry, et al., The effect of composition on the structure of sodium borophosphate glasses, *J. NonCryst. Solids* 354 (31) (2008) 3671–3677, <https://doi.org/10.1016/j.jnoncrysol.2008.04.009>.
- [10] D Larink, H Eckert, M Reichert, SW Martin, Mixed network former effect in ion-conducting alkali borophosphate glasses: Structure/property correlations in the system [M<sub>2</sub>O]<sub>1/3</sub>(B<sub>2</sub>O<sub>3</sub>)<sub>1-x</sub>(P<sub>2</sub>O<sub>5</sub>)<sub>1-x/2/3</sub>(M = Li, K, Cs), *J. Phys. Chem. C* 116 (50) (2012) 26162–26176, <https://doi.org/10.1021/jp307085t>.
- [11] MT Rinke, H. Eckert, The mixed network former effect in glasses: Solid state NMR and XPS structural studies of the glass system (Na<sub>2</sub>O)<sub>x</sub>(BPO<sub>4</sub>)<sub>1-x</sub>, *Phys. Chem. Chem. Phys.* 13 (14) (2011) 6552–6565, <https://doi.org/10.1039/c0cp01590c>.
- [12] D Raskar, MT Rinke, H. Eckert, The mixed-network former effect in phosphate glasses: NMR and XPS structural studies of the connectivity distribution in the glass system (NaPO<sub>3</sub>)<sub>1-x</sub>(B<sub>2</sub>O<sub>3</sub>)<sub>x</sub>, *J. Phys. Chem. C* 112 (2008) 12530–12539, <https://doi.org/10.1039/c0cp01590c>.
- [13] M Zeyer-Diesterer, L Montagne, G Palavit, C. Jäger, Combined <sup>17</sup>O NMR and <sup>11</sup>B-<sup>31</sup>P double resonance NMR studies of sodium borophosphate glasses, *Solid State Nucl. Magn. Reson.* 27 (1–2) (2005) 50–64, <https://doi.org/10.1016/J.SSNMR.2004.06.009>.
- [14] C Hermansen, RE Youngman, J Wang, Y. Yue, Structural and topological aspects of borophosphate glasses and their relation to physical properties, *J. Chem. Phys.* 142 (18) (2015), <https://doi.org/10.1063/1.4919798>.
- [15] C Hermansen, JC Mauro, Y. Yue, A model for phosphate glass topology considering the modifying ion sub-network, *J. Chem. Phys.* 140 (15) (2014), <https://doi.org/10.1063/1.4870764>.
- [16] AC. Wright, Borate structures: crystalline and vitreous, *Phys. Chem. Glasses - Eur. J. Glass Sci. Technol. Part B* 51 (1) (2010) 1–39.
- [17] I Ahmed, M Lewis, I Olsen, JC. Knowles, Phosphate glasses for tissue engineering: Part 1. Processing and characterisation of a ternary-based P<sub>2</sub>O<sub>5</sub>-CaO-Na<sub>2</sub>O glass system, *Biomaterials* 25 (3) (2004) 501–507, [https://doi.org/10.1016/S0142-9612\(03\)00547-7](https://doi.org/10.1016/S0142-9612(03)00547-7).
- [18] I Ahmed, M Lewis, I Olsen, JC. Knowles, Phosphate glasses for tissue engineering: Part 2. Processing and characterisation of a ternary-based P<sub>2</sub>O<sub>5</sub>-CaO-Na<sub>2</sub>O glass fibre system, *Biomaterials* 25 (3) (2004) 501–507, [https://doi.org/10.1016/S0142-9612\(03\)00547-7](https://doi.org/10.1016/S0142-9612(03)00547-7).
- [19] MT Islam, RM Felfel, EA Abou Neel, DM Grant, I Ahmed, KMZ Hossain, Bioactive calcium phosphate-based glasses and ceramics and their biomedical applications: A review, *J Tissue Eng* 8 (2017) 1–16, <https://doi.org/10.1177/2041731417719170>.
- [20] SM Abo-Naf, ESM Khalil, ESM El-Sayed, HA Zayed, RA. Youness, In vitro bioactivity evaluation, mechanical properties and microstructural characterization of Na<sub>2</sub>O-CaO-B<sub>2</sub>O<sub>3</sub>-P<sub>2</sub>O<sub>5</sub> glasses, *Spectrochimica Acta - Part A* 144 (2015) 88–98, <https://doi.org/10.1016/j.saa.2015.02.076>.
- [21] A Saranti, I Koutselas, MA. Karakassides, Bioactive glasses in the system CaO-B<sub>2</sub>O<sub>3</sub>-P<sub>2</sub>O<sub>5</sub>: Preparation, structural study and in vitro evaluation, *J. NonCryst. Solids* 352 (5) (2006) 390–398, <https://doi.org/10.1016/j.jnoncrysol.2006.01.042>.
- [22] A Wren, D Boyd, MR. Towler, The processing, mechanical properties and bioactivity of strontium based glass polyalkenoate cements, *J. Mater. Sci. Mater. Med.* 19 (4) (2008) 1737–1743, <https://doi.org/10.1007/s10856-007-3287-z>.
- [23] E Gentleman, YC Fredholm, G Jell, et al., The effects of strontium-substituted bioactive glasses on osteoblasts and osteoclasts in vitro, *Biomaterials* 31 (14) (2010) 3949–3956, <https://doi.org/10.1016/j.biomaterials.2010.01.121>.
- [24] C Wu, Y Ramaswamy, D Kwik, H. Zreiqat, The effect of strontium incorporation into CaSiO<sub>3</sub> ceramics on their physical and biological properties, *Biomaterials* 28 (21) (2007) 3171–3181, <https://doi.org/10.1016/J.BIOMATERIALS.2007.04.002>.
- [25] J Lao, E Jallot, JM. Nedelec, Strontium-delivering glasses with enhanced bioactivity: A new biomaterial for antioestrogenic applications? *Chem. Mater.* 20 (15) (2008) 4969–4973, <https://doi.org/10.1021/cm800993s>.
- [26] PT Freudenberger, A Saitoh, H Ikeda, et al., Characterization of 20Na<sub>2</sub>O-30(1-x)CaO-xSrO)-50P<sub>2</sub>O<sub>5</sub> glasses for a resorbable optical fiber application, *Int. J. Appl. Glass Sci.* 10 (3) (2019), <https://doi.org/10.1111/ijag.13106>.
- [27] T Jin, GM Bernard, M Miskolzie, V v. Terskikh, VK. Michaelis, A <sup>11</sup>B and <sup>31</sup>P MAS NMR study of the impact of Ca<sup>2+</sup> and Sr<sup>2+</sup> network modifying cations on the structure of borate and borophosphate glasses, *Phys. Chem. Glasses* 59 (4) (2018) 174–180, <https://doi.org/10.13036/17533562.59.4.048>.
- [28] Q Jiang, H Zeng, Z Liu, et al., Glass transition temperature and topological constraints of sodium borophosphate glass-forming liquids, *J Chem Phys* 139 (2013), 124502, <https://doi.org/10.1063/1.4821617>.
- [29] Freudenberger PT, Blatt RL, Youngman RE, Brow RK. Dissolution Behavior of Borophosphate Glasses in Deionized Water and Simulated Body Fluid. *in preparation*. 2021.
- [30] BC Sales, LA Boatner, JO. Ramey, Chromatographic studies of the structures of amorphous phosphates: a review, *J. NonCryst. Solids* 263–264 (2000) 155–166, [https://doi.org/10.1016/S0022-3093\(99\)00644-4](https://doi.org/10.1016/S0022-3093(99)00644-4).
- [31] D Massiot, F Fayon, M Capron, et al., *Magn Reson Chem* 40 (2002) 70–76.
- [32] D Massiot, C Bessada, J Coutures, F. Taulelle, A quantitative study of <sup>27</sup>Al MAS NMR in crystalline YAG, *J.f Magnetic Resonance* (1969) 90 (2) (1990) 231–242.
- [33] JJ Hudgens, SW. Martin, Glass transition and infrared spectra of low-alkali, anhydrous lithium phosphate glasses, *J. Am. Ceram. Soc.* 76 (7) (1993) 1691–1696, <https://doi.org/10.1111/j.1151-2916.1993.tb06636.x>.
- [34] JF Duclé, JJ. Videau, Structural study of borophosphate glasses by Raman and infrared spectroscopy, *Phys. Chem. Glasses* 34 (5) (1993) 212–218.
- [35] El Kamitsos, GD. Chryssikos, Borate glass structure by Raman and infrared spectroscopies, *J. Mol. Struct.* 247 (1991) 1–16, [https://doi.org/10.1016/0022-2860\(91\)87058-P](https://doi.org/10.1016/0022-2860(91)87058-P).
- [36] WL Konijnendijk, JM. Stevels, The Structure of Borate Glasses Studied by Raman Scattering, *J. NonCryst. Solids* 18 (1975) 307–331.
- [37] D Maniua, T Iliescu, I Ardelean, S Cinta-Pinzaru, N Tarcea, W. Kiefer, Raman study on B<sub>2</sub>O<sub>3</sub>-CaO glasses, *J. Mol. Struct.* 651–653 (2003) 485–488, [https://doi.org/10.1016/S0022-2860\(03\)00129-7](https://doi.org/10.1016/S0022-2860(03)00129-7). Elsevier.
- [38] M Scagiotti, M Villa, G. Chioldelli, Short range order in the network of the borophosphate glasses: Raman results, *J. NonCryst. Solids* 93 (2–3) (1987) 350–360, [https://doi.org/10.1016/S0022-3093\(87\)80180-1](https://doi.org/10.1016/S0022-3093(87)80180-1).

- [39] JJ Hudgens, RK Brow, DR Tallant, SW. Martin, Raman spectroscopy study of the structure of lithium and sodium ultraphosphate glasses, *J. NonCryst. Solids* 223 (1–2) (1998) 21–31, [https://doi.org/10.1016/S0022-3093\(97\)00347-5](https://doi.org/10.1016/S0022-3093(97)00347-5).
- [40] RK. Brow, Review: the structure of simple phosphate glasses, *J. NonCryst. Solids* 263–264 (2000) 1–28, [https://doi.org/10.1016/S0022-3093\(99\)00620-1](https://doi.org/10.1016/S0022-3093(99)00620-1).
- [41] BC Sales, RS Ramsey, JB Bates, LA. Boatner, Investigation of the structural properties of lead-iron phosphate glasses using liquid chromatography and raman scattering spectroscopy, *J. NonCryst. Solids* 87 (1986) 137–158.
- [42] UP Strauss, TL. Treitler, Degradation of polyphosphates in solution. I. Kinetics and mechanism of the hydrolysis at branching points in polyphosphate chains, *J Am Chem Soc* 78 (15) (1956) 3553–3557, <https://doi.org/10.1039/j3970000X001>.
- [43] L Muñoz-Senovilla, G Tricot, F. Muñoz, Kinetic fragility and structure of lithium borophosphate glasses analysed by 1D/2D NMR, *Phys. Chem. Chem. Phys.* 19 (34) (2017) 22777–22784, <https://doi.org/10.1039/c7cp04171c>.
- [44] RK Brow, CA Click, TM. Alam, Modifier coordination and phosphate glass networks, *J. NonCryst. Solids* 274 (2000) 9–16.
- [45] M Villa, M Scagliotti, G. Chiodelli, Short range order in the network of the borophosphate glasses: a  $^{31}\text{P}$  NMR-MAS (Magic Angle Spinning) study, *J. NonCryst. Solids* 94 (1) (1987) 101–121, [https://doi.org/10.1016/S0022-3093\(87\)80264-8](https://doi.org/10.1016/S0022-3093(87)80264-8).
- [46] JL Miquel, L Facchini, AP Legrand, C Rey, J. Lemaitre, Solid state NMR to study calcium phosphate ceramics, *Colloids Surf.* 45 (C) (1990) 427–433, [https://doi.org/10.1016/0166-6622\(90\)80041-2](https://doi.org/10.1016/0166-6622(90)80041-2).
- [47] S Hayakawa, K Tsuru, H Iida, C Ohtsuki, A. Osaka,  $^{31}\text{P}$  MAS-NMR studies of phosphate salts formation on calcium-containing oxide glasses in a simulated body fluid, *J. Ceram. Soc. Jpn.* 104 (11) (1996) 1000–1003, <https://doi.org/10.2109/jcersj.104.1000>.
- [48] RJB Jakeman, AK Cheetham, NJ Clayden, CM. Dobson, A magic angle spinning NMR study of the phase diagram  $\text{Ca}_3\text{-xZn}_x(\text{PO}_4)_2$ , *J. Solid State Chem.* 78 (1) (1989) 23–34, [https://doi.org/10.1016/0022-4596\(89\)90124-2](https://doi.org/10.1016/0022-4596(89)90124-2).
- [49] AR Grimmer, D Müller, G Gözel, R. Kniep, Multinuclear ( $^{11}\text{B}$ ,  $^{31}\text{P}$ ) MAS NMR spectroscopy of borophosphates, *Fresenius J Anal Chem* 357 (5) (1997) 485–488, <https://doi.org/10.1007/s002160050197>.
- [50] MM. Smedskjaer, Structural and Topological Basis of Glass Properties and Diffusion, Aalborg University, 2011.
- [51] MM Smedskjaer, JC Mauro, RE Youngman, CL Hogue, M Potuzak, Y. Yue, Topological principles of borosilicate glass chemistry, *J Phys Chem B* 115 (2011) 12930–12946, <https://doi.org/10.1021/jp208796b>.
- [52] CJ Wilkinson, Q Zheng, L Huang, JC. Mauro, Topological constraint model for the elasticity of glass-forming systems, *J. Non-Cryst. Solids: X* 2 (2019), 100019, <https://doi.org/10.1016/J.NOCX.2019.100019>.
- [53] C Hermansen, X Guo, RE Youngman, JC Mauro, MM Smedskjaer, Y. Yue, Structure-topology-property correlations of sodium phosphosilicate glasses, *J. Chem. Phys.* 143 (6) (2015), <https://doi.org/10.1063/1.4928330>.
- [54] S Elbers, W Strojek, L Koudelka, H. Eckert, Site connectivities in silver borophosphate glasses: new results from  $^{11}\text{B}\{^{31}\text{P}\}$  and  $^{31}\text{P}\{^{11}\text{B}\}$  rotational echo double resonance NMR spectroscopy, *Solid State Nucl. Magn. Reson.* 27 (1–2) (2005) 65–76, <https://doi.org/10.1016/j.ssnmr.2004.08.007>.
- [55] B Tischendorf, JU Otaigbe, JW Wiench, M Pruski, BC. Sales, A study of short and intermediate range order in zinc phosphate glasses, *J. NonCryst. Solids* 282 (2–3) (2001) 147–158, [https://doi.org/10.1016/S0022-3093\(01\)00350-7](https://doi.org/10.1016/S0022-3093(01)00350-7).
- [56] F Döhler, A Mandlule, L van Wüllen, M Friedrich, DS. Brauer,  $^{31}\text{P}$  NMR characterisation of phosphate fragments during dissolution of calcium sodium phosphate glasses, *J Mater Chem B* 3 (6) (2015) 1125–1134, <https://doi.org/10.1039/c4tb01757a>.
- [57] L Ma, RK. Brow, Structural study of  $\text{Na}_2\text{O-FeO-Fe}_2\text{O}_3\text{-P}_2\text{O}_5$  glasses by high-pressure liquid chromatography, *J. NonCryst. Solids* 387 (2014) 16–20, <https://doi.org/10.1016/j.jnoncrysol.2013.12.011>.
- [58] Ma L, Brow K, Schlesinger ME. Dissolution behaviour of sodium calcium polyphosphate glasses. 2018;59(5):205–212. doi:10.13036/17533562.59.5.018.
- [59] BC Sales, JU Otaigbe, GH Beall, LA Boatner, JO. Ramey, Structure of zinc polyphosphate glasses, *J. NonCryst. Solids* 226 (3) (1998) 287–293, [https://doi.org/10.1016/S0022-3093\(98\)00415-3](https://doi.org/10.1016/S0022-3093(98)00415-3).
- [60] B Wang, BS Kwak, BC Sales, JB. Bates, Ionic conductivities and structure of lithium phosphorus oxynitride glasses, *J. NonCryst. Solids* 183 (3) (1995) 297–306, [https://doi.org/10.1016/0022-3093\(94\)00665-2](https://doi.org/10.1016/0022-3093(94)00665-2).
- [61] P Zapol, H He, KD Kwon, LJ. Criscenti, First-principles study of hydrolysis reaction barriers in a sodium borosilicate glass, *Int. J. Appl. Glass Sci.* 4 (4) (2013) 395–407, <https://doi.org/10.1111/ijag.12052>.
- [62] G Geneste, F Bouyer, S. Gin, Hydrogen-sodium interdiffusion in borosilicate glasses investigated from first principles, *J. NonCryst. Solids* 352 (28–29) (2006) 3147–3152, <https://doi.org/10.1016/j.jnoncrysol.2006.04.023>.
- [63] KL Goetschius, MA Beuerlein, CM Bischo, RK. Brow, Dissolution behavior of ternary alkali-alkaline earth-borate glasses in water, *J. NonCryst. Solids* 487 (2018) 12–18, <https://doi.org/10.1016/j.jnoncrysol.2018.02.011>.
- [64] JR. Van Wazer, Phosphorus and its Compounds, Interscience, New York, NY, 1958.
- [65] D Qiu, P Guerry, I Ahmed, et al., A high-energy X-ray diffraction,  $^{31}\text{P}$  and  $^{11}\text{B}$  solid-state NMR study of the structure of aged sodium borophosphate glasses, *Mater. Chem. Phys.* 111 (2–3) (2008) 455–462, <https://doi.org/10.1016/j.matchemphys.2008.04.045>.
- [66] G Tricot, B Raguenet, Silly, et al., P-O-B<sup>3</sup> linkages in borophosphate glasses evidenced by high field  $^{11}\text{B}/^{31}\text{P}$  correlation NMR, *Chem. Commun.* 51 (2015) 9284–9286.